Skin Penetration and Cellular Uptake of Amorphous Silica Nanoparticles with Variable Size, Surface Functionalization, and Colloidal Stability

Fiorenza Rancan,[†,*] Qi Gao,[‡] Christina Graf,[‡,*] Stefan Troppens,[†,⊥] Sabrina Hadam,[†] Steffen Hackbarth,[§] Cynthia Kembuan,[‡] Ulrike Blume-Peytavi,[†] Eckart Rühl,[‡] Jürgen Lademann,[⊥] and Annika Vogt[†]

[†]Clinical Research Center for Hair and Skin Science, Department of Dermatology and Allergy and [⊥]Center of Experimental and Applied Cutaneous Physiology, Department of Dermatology and Allergy, Charité-Universitätsmedizin Berlin, Berlin, Germany, [‡]Physikalische Chemie, Institut für Chemie und Biochemie Freie Universität Berlin, Germany, and [§]Photobiophysik, Institut für Physik, Humboldt Universität Berlin, Berlin, Germany

ABSTRACT In this study, the skin penetration and cellular uptake of amorphous silica particles with positive and negative surface charge and sizes ranging from 291 ± 9 to 42 ± 3 nm were investigated. Dynamic light scattering measurements and statistical analyses of transmission electron microscopy images were used to estimate the degree of particle aggregation, which was a key aspect to understanding the results of the *in vitro* cellular uptake experiments. Despite partial particle aggregation occurring after transfer in physiological media, particles were taken up by skin cells in a size-dependent manner. Functionalization of the particle surface with positively charged groups enhanced the *in vitro* cellular uptake. However, this positive effect was contrasted by the tendency of particles to form aggregates, leading to lower internalization ratios especially by primary skin cells. After topical application of nanoparticles on human skin explants with partially disrupted stratum corneum, only the 42 ± 3 nm particles were found to be associated with epidermal cells and especially dendritic cells, independent of their surface functionalization. Considering the wide use of nanomaterials in industries and the increasing interest for applications in pharmaceutics and cosmetics versus the large number of individuals with local or spread impairment of the skin barrier, *e.g.*, patients with atopic dermatitis and chronic eczema, a careful dissection of nanoparticle-skin surface interactions is of high relevance to assess possible risks and potentials of intended and unintended particle exposure.

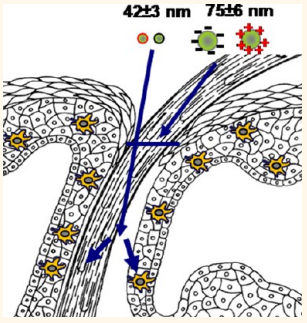

KEYWORDS: amorphous silica nanoparticles · colloidal stability · skin penetration · HaCaT cells · keratinocytes · dendritic cells

A number of commercially available products, including food, drugs, cosmetics, and textiles already contain nanoparticles as active agents, carriers, or additives. Nanoparticles are currently explored in several fields including materials science as well as biomedical research.[1] In dermatology and cosmetology nanoparticles promise to become important tools for a more efficient and selective targeting of drugs to skin regions and cell populations of interest.[2] However, up to now, little is known about the principles underlying nanoparticle translocation through body barriers as well as the mechanisms of cellular uptake of particles and their possible interactions with biological processes. In addition, the former hypothesis that nanoparticles made of nontoxic material would be harmless has been already replaced by the evidence that nanoparticles can interact with several biological systems in a different way than the corresponding bulk material does. Indeed, it has been shown that several materials in their particulate state, and especially in the nanometer range, can become toxic.[3−5] Improved understanding of how the physicochemical properties can influence nanoparticle interactions with biological systems is needed to ensure an efficient and safe use of nanosized materials.

Besides lung and gut, skin is one of the major entry routes for external substances, especially because of its large surface area and accessibility to environmental exposure. Nanoparticle contact with skin may happen accidentally but also intentionally because of their presence in clothing, drugs, cosmetics, and other skin care products. Healthy skin is an efficient barrier to the external environment, protecting the body from dangerous pathogens and substances. A first physical barrier is represented by the lipid extracellular matrix and several layers of terminally differentiated cornified cells, called Stratum Corneum (SC), as well as by sebum and sweat produced by skin appendages. In addition, directly beneath the SC, tight junctions seal the apical intercellular spaces between the cells of the viable

* Address correspondence to fiorenza.rancan@charite.de, cmgraf@zedat.fu-berlin.de.

Received for review April 13, 2012 and accepted July 13, 2012.

Published online July 13, 2012
10.1021/nn301622h

epidermis. A further barrier is represented by the network of antigen presenting cells in the epidermis and dermis, which have the role to recognize and process penetrating foreign materials and organisms and to elicit immune responses.[6] Most of the studies assessing the skin penetration of different nanoparticle types after topical application have shown penetration of particles into upper layers of the SC but not deeper into the viable epidermis and dermis. Lademann and coworkers have shown that after repeated applications of an oil/water emulsion to human volunteers, 17 nm titanium dioxide nanoparticles penetrated only to the upper SC and accumulated in hair follicles canals.[7] Even smaller iron nanoparticles (10 nm) were shown to accumulate in hair follicle orifices and penetrate through the lipid matrix of the SC but were never detected deeper than the uppermost strata of the epidermis.[8] Similarly, ZnO nanoparticles (26−30 nm)[9] and nail-shaped quantum dots coated with carboxylic acid[10] have been reported to penetrate not deeper than the SC. Polyvinylpyrrolidone-coated silver nanoparticles (25 ± 7.1 nm) were detected by means of transmission electron microscopy (TEM) in the SC and only in the upper keratinocyte layers.[11] Nevertheless, there is strong evidence that the extent of nanoparticle penetration into the skin changes, when the integrity of the skin barrier is altered and the immune system is activated. In fact, there are a few studies, which report on nanoparticle skin penetration across a damaged skin barrier using different skin models.[12−14] In our previous investigations, we showed that polystyrene nanoparticles could translocate to the viable epidermis using human skin explants pretreated with cyanoacrylate skin surface stripping (CSSS), which induces mild barrier disruption, but also opens hair follicle orifices for shunt penetration.[12] In later studies on mice, the relevance of such shunt penetration was demonstrated on murine skin, where particles could be tracked in hair follicles, in the surrounding dermis, and, subsequently, in draining lymph nodes and secondary lymphatic organs upon cutaneous application.[13] Using UV irradiated skin as another model for altered skin barrier, Mortensen *et al.* reported on quantum dot translocation to the viable skin of mice.[14]

In this study, we used the CSSS-pretreated human skin explants to compare amorphous silica particles of different sizes and surface charges with regard to skin penetration and cellular uptake. Silica particles have several industrial applications because of their specific properties such as abrasion resistance, chemical inertness, and high thermal stability. They are used as additives, fillers, and a rheological modifier for food, cosmetics, paints, and other products.[5] Furthermore, silica particles are investigated as drug carrier systems for medical use[15] and are widely used as model systems due to the numerous surface functionalization possibilities.[16−18] A number of toxicological data have been reported about crystalline silica,[19] but significantly less *in vivo* studies on the biological effects of amorphous colloidal silica have been published. Toxicity data have been obtained in mice after intravenous[5] and gastrointestinal administration of particles.[20] The induction of inflammatory responses was found in mice after administration of acute or subacute doses *via* the respiratory tract.[21] Surprisingly, there is only one published work reporting on *in vivo* investigations on skin penetration and toxicity of amorphous silica particles after topical administration.[22] Therefore, many questions about silica particle interaction with skin remain unsolved, and substantially improved knowledge on silica nanoparticles translocation through the skin barrier and cellular uptake is still needed.

One of the main problems, encountered when investigating the interactions of micro- and nanoparticles with biological materials, is the instability of the colloidal dispersions in physiological media and the consequent particle aggregation. Even particles which can be well dispersed in different organic solvents or water, often aggregate when they are transferred to physiological media.[23] This effect is due to the ionic strength and polarity of the used dispersing phase but might also result from complex interactions between the functionalization groups on the surface of the particles and the components of the media, for example, phosphates.[23] On the one hand, particle aggregation in both *in vitro* and *in vivo* conditions might reduce the number of nonaggregated particles available for interactions with biological membranes and cellular uptake. On the other hand, aggregation occurring in certain body compartments or inside cells could give rise to novel cytotoxic effects.[24] To evaluate the effect of particle aggregation on their cellular uptake and skin penetration we investigated the colloidal stability of the particles in those physiological media which were used during the experiments. These results allowed us to provide more detailed information on the extent of particle aggregation during the experiments using both isolated cells and human skin explants.

RESULTS AND DISCUSSION

Preparation and Colloidal Stability of Silica Particles after Transfer into Physiological Media. Fluoresceine isothiocyanate (FITC)-labeled silica particles of four different sizes were prepared by a seeded growth process. First, a silica core covalently labeled with FITC was synthesized by a microemulsion synthesis. Subsequently, up to four additional layers of silica were grown on these particles in a Stöber-like growth process.[25−28] The resulting particles had an outermost dye-free silica layer of about 3 nm thickness, so that any interaction of dye molecules with the surrounding physiological medium could be excluded. Spherical particles with diameters

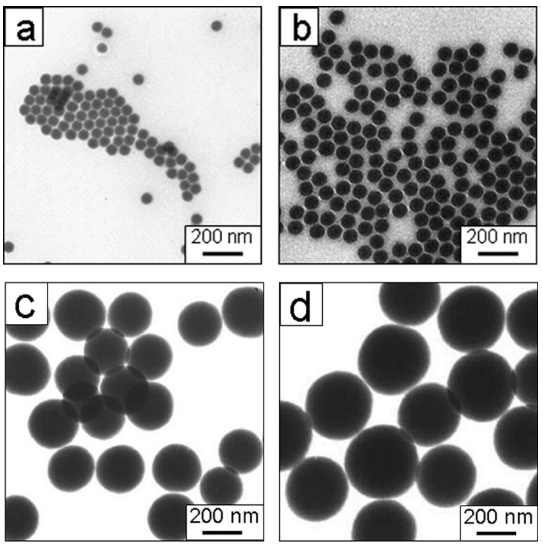

Figure 1. TEM images of APS-functionalized silica nanoparticles of the samples SiO_2-42 (a), SiO_2-75 (b), SiO_2-200(c), and SiO_2-300 (d).

TABLE 1. Diameter Measured by TEM and DLS as well as Zeta Potential of Silica Particles without Surface Functionalization in Water (pH = 7)

sample	TEM[a] diameter (nm)	DLS diameter (nm)	zeta potential (mV)
SiO_2-42	42 ± 3	110 ± 3	- 22 ± 3
SiO_2-75	75 ± 6	101 ± 7	- 45 ± 4
SiO_2-200	190 ± 9	206 ± 16	- 56 ± 5
SiO_2-300	291 ± 9	331 ± 19	- 48 ± 2

[a] TEM data are obtained from particle ethanolic dispersions after the evaporation of the dispersing phase.

of 42 ± 3 nm (sample SiO_2-42), 75 ± 6 nm (sample SiO_2-75), 190 ± 9 nm (sample SiO_2-200), and 291 ± 9 nm (sample SiO_2-300) were produced with low polydispersity, as measured by TEM (see Figure 1a–d).

These particles were colloidally stable in ethanol and water. The colloidal stability in water was confirmed by additional measurements of their hydrodynamic diameter, as determined by dynamic light scattering (see Table 1). These data indicate that the particles were only slightly larger in water than the particles dried from ethanol. Further, they had a relatively high negative zeta potential (see Table 1). Only particles of the sample SiO_2-42 had a zeta potential with an absolute value that was lower than −30 mV, where −22 ± 3 mV were found. As a consequence of this low surface charge some aggregates were formed, which resulted in a more than doubled hydrodynamic diameter compared to the corresponding value for the dried particles measured by TEM (see Table 1). *In vitro* studies with cultured cells, however, usually require transfer of particles in physiological media, which causes alterations of the surface charge and the colloidal stability. This aspect has to be considered in the design of such experiments. In fact,

TABLE 2. Hydrodynamic Diameter and Zeta Potential of Silica Particles without Surface Functionalization in PBS (pH = 7.4) Directly and 1 Week after Transfer in the Medium

	directly after transfer		1 week after transfer	
sample[a]	DLS diameter (nm)	zeta potential (mV)	DLS diameter (nm)	zeta potential (mV)
SiO_2-42	1000 ± 100	−2 ± 1	2000 ± 200	−1.0 ± 1.3
SiO_2-75	1000 ± 100	−2 ± 1	3800 ± 400	−0.7 ± 1.5
SiO_2-200	2000 ± 300	−1 ± 2	4900 ± 500	−0.3 ± 1.2

[a] The SiO_2-300 sample aggregates and precipitates in PBS, hence no proper DLS or zeta potential measurements are possible.

when the particles are incubated in physiological buffers or cell culture media their zeta potential and degree of aggregation will be changed depending on the ionic strength, pH, and other properties of the dispersing medium.[23,29−31] Further, the aggregation of silica nanoparticles is highly sensitive to the transfer process from ethanol to physiological media.[23] Thus, nanoparticles added to physiological media or biological systems are typically partially aggregated already before they come in contact with cell membranes. Therefore, the detailed analysis of such aggregated systems is of primary importance in order to investigate the influence of size and surface functionalization on cellular uptake and skin penetration. In this study, we developed a transfer protocol which led to a reproducible partial particle aggregation. The ethanolic particle dispersion was diluted with PBS, and centrifuged and redispersed in PBS twice in order to ensure that <0.5 vol. % of ethanol was present in the samples. The extent of particle aggregation after this transfer protocol was studied by means of TEM and dynamic light scattering. After this transfer procedure, the zeta potential of the investigated particles had only a value between −1 and −2 mV and consequently aggregation occurred, which resulted in hydrodynamic diameters of about 1000 nm or even larger values for the samples SiO_2-42, SiO_2-75, and SiO_2-200 (see Table 2). The sample SiO_2-300 partially precipitated, and consequently, proper zeta potential and light scattering measurements were impeded. The aggregation slowly progressed with time and after 1 week of storage in PBS the hydrodynamic diameters were 2–4 times larger than directly after transfer (see Table 2). The aggregates could not be redispersed by diluting with PBS or treating them with ultrasound. The reduced colloidal stability in PBS can be explained by the high salt content and the resulting ionic strength of PBS (I_s = 0.174 mol/L) which reduces the thickness of the electrostatic double layer and hence, the colloidal stability of the nanoparticles.[23,32−34]

All particles were first transferred and stored in PBS and then added as dispersion in PBS to the cells

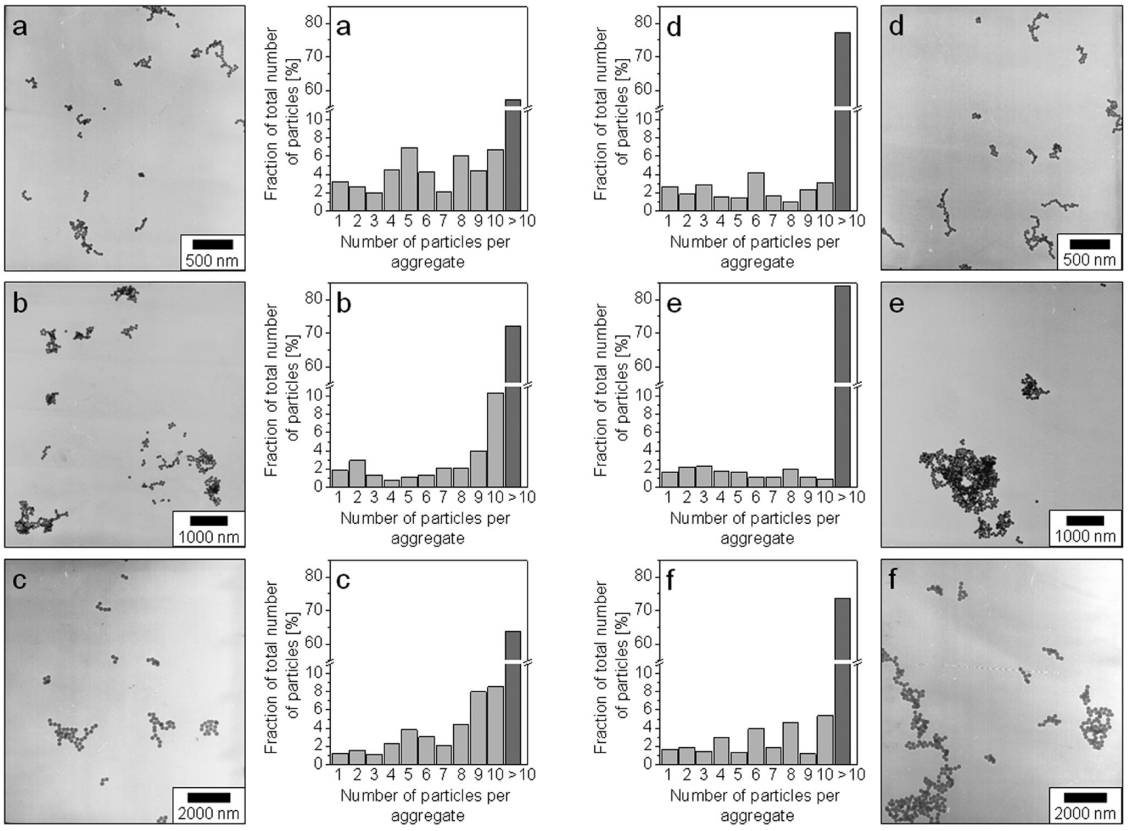

Figure 2. TEM analysis of the aggregated silica nanoparticles without and with surface functionalization after their transfer in PBS (pH 7.4). Results of the statistical analysis and representative TEM images of the corresponding samples (a) SiO_2-42, (b) SiO_2-75, (c) SiO_2-200, (d) APS-SiO_2-42, (e) APS-SiO_2-75, and (f) APS-SiO_2-200 are displayed.

obtaining a thousand fold dilution of the particles in the cell culture medium RPMI-1640. In RPMI-1640 the particles were highly diluted (c = 0.01 g/L). Hence, a proper modeling of the evolution of the particle aggregation in RPMI-1640 by DLS measurements was not possible. We have recently shown that at least concentrated samples (c = 0.55 g/L) have in RPMI-1640 a hydrodynamic diameter about 1.5 times larger than in PBS.[23] Consequently, the results obtained from studies in PBS give a lower limit of the average hydrodynamic diameter of the particles during the cellular uptake experiments. The hydrodynamic diameters were obtained from a cumulant fit of dynamic light scattering data and are consequently average values for a large number of particles. As the light scattering measurements were carried out at only one fixed scattering angle of 165°, it has to be taken into account that the obtained particle diameters are sufficiently accurate for small silica nanoparticles (<100 nm), whereas for larger aggregates, with size of the order of the incident wavelength, the angular-dependence of the scattered light has to be considered, as well.[35] Intensity measurements at small angles are known to be more sensitive to the growth of aggregates during the coagulation process than measurements at large scattering angles. Therefore, the average size of the aggregates is likely underestimated by this simple approach, which makes use of a fixed scattering angle.[35] Nevertheless, a large average hydrodynamic diameter obtained from DLS measurements does not imply that only aggregates are present in the sample. The scattering intensity is proportional to the sixth power of the diameter of the scatterer; consequently, small particles are practically not detected in such measurements. In contrast, TEM allows us to visualize single nanoparticles as well as small aggregates if drying effects are negligible. Therefore, a statistical analysis of the samples SiO_2-42, SiO_2-75, and SiO_2-200 was carried out. The samples were highly diluted with PBS in order to minimize the drying effects. DLS data indicate that dilution of the samples does not change the state of aggregation, so that it is assumed that the extent of particle aggregation corresponds to that of the nanoparticle dispersions used for the uptake experiments. Representative TEM images of each sample are displayed in Figures 2a–c and reveal that nonaggregated particles and small aggregates were still present in all samples.

The results of the statistical analysis are also shown in Figure 2. In the case of sample SiO_2-42, a fraction of about 43% of all particles corresponded to nonaggregated particles or small aggregates (aggregation number ≤10, see Figure 2a). More than half of the particles were found in larger aggregates, with aggregation

TABLE 3. Particle Diameters Obtained from TEM and DLS Measurements As Well As Zeta Potential of Silica Particles Functionalized with APS in Water (pH = 7)

sample	TEM diameter (nm)	DLS diameter (nm)	zeta potential (mV)
APS-SiO_2-42	42 ± 3	121 ± 4	+12 ± 2
APS-SiO_2-75	75 ± 6	122 ± 7	+11 ± 3
APS-SiO_2-200	190 ± 9	235 ± 12	+10 ± 1
APS-SiO_2-300	291 ± 9	326 ± 16	+10 ± 2

numbers reaching up to a few hundred particles. The smaller nanoparticle aggregates had often a chain-like structure, whereas the larger ones were fractal structures, which is typical for reaction limited colloidal aggregation.[36] In the sample SiO_2-75 the fraction of nonaggregated particles and small aggregates with an aggregation number ≤10 was significantly smaller (about 28%) than in sample SiO_2-42 and, among those, most of the aggregates contained 9 or 10 particles (Figure 2b). Sample SiO_2-200 contained less aggregates than sample SiO_2-75; about 36% of the particles had an aggregation number ≤10 (Figure 2c). However, the average hydrodynamic diameter of sample SiO_2-200 in PBS was twice as large as that of sample SiO_2-75 (see Table 2), which is due to the larger diameter of the primary particles of sample SiO_2-200 (approximately 2.5 fold with respect to SiO_2-75, see Table 1).

The initial step of the interaction between nanoparticles and cells is particle adsorption on the cell membrane, which is followed by the uptake into the interior of the cell.[37] As the cell membrane has several negatively charged groups,[37] it is expected that positively charged nanoparticles are taken up better than negatively charged ones. To investigate the influence of a positive surface charge with regard to silica particle cellular uptake and penetration into skin, (3-aminopropyl)-trimethoxysiliane (APS) was covalently bound on the silica surface of the four above-mentioned particle sizes. These samples are named APS-SiO_2-42, APS-SiO_2-75, APS-SiO_2-200, and APS-SiO_2-300, respectively. APS is often used to functionalize silica particles for *in vivo* and *in vitro* studies.[38−42] TEM measurements confirmed that the diameter and the morphology of the nanoparticles were unchanged after this surface modification. In addition, zeta potential measurements confirmed that the particle charge was converted from negative to positive (see Table 3). However, the absolute value of the zeta potential in water was relatively low (+10 to +12 mV), implying that the colloidal stability of the particles was modest. This can be explained by a slow detachment of the APS ligands from the silica particles in aqueous dispersion, which is promoted by the formation of a stable cyclic intermediate.[23,43] As a result of the lower colloidal stability, the hydrodynamic diameter of the nanoparticles was increased compared to the diameter measured by TEM. Note that the diameters of the larger

TABLE 4. Hydrodynamic Diameter and Zeta Potential of Silica Particles Functionalized with APS in PBS (pH = 7.4) Directly and 1 Week after Transfer in the Medium

	directly after transfer		1 week after transfer	
sample[a]	DLS diameter (nm)	zeta potential (mV)	DLS diameter (nm)	zeta potential (mV)
APS-SiO_2-42	1600 ± 100	+4 ± 1	2300 ± 200	+0.6 ± 1.1
APS-SiO_2-75	2100 ± 100	+2 ± 2	3900 ± 400	+0.8 ± 1.5
APS-SiO_2-2 0	3400 ± 200	+1 ± 2	5000 ± 800	−0.2 ± 1.3

[a] The APS-SiO_2-300 sample aggregates and precipitates in PBS, hence no proper DLS or zeta potential measurements are possible.

particles (APS-SiO_2-200 and APS-SiO_2-300) were only slightly increased with respect to particle primary size, whereas the APS-SiO_2-75 particles had a more than 60% larger diameter and the hydrodynamic diameter of the APS-SiO2-42 sample was almost three times larger than the value obtained from TEM. These values are still similar to the corresponding hydrodynamic diameters of the nonfunctionalized particles in water (see Table 1). The transfer of the APS-SiO_2-42, APS-SiO_2-75, and APS-SiO_2-200 samples in PBS resulted in a significant decrease of the zeta potential, which reached only values about +1 to +4 mV (see Table 4). Consequently, these particles strongly aggregated, and average hydrodynamic diameters of about 1600−3400 nm were measured (see Table 4). Similar to the results obtained for the nonfunctionalized particles, the extent of aggregation increased when the particles were stored for 1 week in PBS. Also the zeta potential was further decreased and reaches values around zero after this time period (see Table 4). In a detailed study on the aggregation kinetics of APS-functionalized 55 nm diameter silica particles, we could recently show that by using an optimized transfer protocol (see Materials and Methods section), the initial zeta potential and the hydrodynamic diameter are only slightly lower than in water.[23] However, also in this case severe aggregation occurred within 16 h after transfer due to the detachment of APS ligands from the particle surface in aqueous environment, as explained above.[23] The particles of sample APS-SiO_2-300 aggregated and partially precipitated and, hence, could not be further characterized by DLS and zeta potential measurements in PBS. The statistical analysis of TEM images of at least 3700 particles per sample revealed that the three samples still contained a significant number of nonaggregated nanoparticles and small aggregates, despite the large average hydrodynamic diameters (Figure 2d−f). About 23% of the particles of APS-SiO_2-42 sample were nonaggregated particles or small aggregates (aggregation number ≤10, see Figure 2d). This is a significant smaller fraction with respect to that found for the corresponding nonfunctionalized SiO_2-42 samples, in which about 43% of the particles were not aggregated or formed small aggregates (Figure 2a).

This result agrees well with the increased hydrodynamic diameter of sample APS-SiO_2-42 in PBS (1600 ± 100 nm) as compared to sample SiO_2-42 in PBS (1000 ± 1 00 nm). In sample APS-SiO_2-75, the fraction of particles with aggregation number ≤10 was even smaller: less than 16% (Figure 2e). Most of the particles were forming large aggregates with aggregation numbers up to 700 (Figure 2e). These are the largest aggregation numbers found for all samples in the present work. A typical example for such a large aggregate is displayed in Figure 2e. Also in the case of sample APS-SiO_2-75 the fraction of particles with aggregation number ≤10 was smaller than that found for the corresponding nonfunctionalized sample SiO_2-75, (28%, Figure 2b). In sample APS-SiO_2-200 about 26% of the particles had an aggregation number ≤10 (Figure 2f), compared to 36% in the corresponding nonfunctionalized sample SiO_2-200 (Figure 2c). The results obtained from the statistical analysis of TEM images are in full agreement with the data obtained with dynamic light scattering, yielding for all APS-functionalized particles significantly larger average hydrodynamic diameters than for the corresponding particles without an APS functionalization (see Tables 2 and 4). Furthermore, the statistical analysis of particle TEM images allows obtaining more detailed information about the number of nonaggregated particles and small aggregates that are effectively available during the cellular uptake and skin penetration experiments and are very useful for the interpretation of the cellular uptake experiments.

Positive surface charge enhances particle uptake by HaCaT cells. The cell line HaCaT was first used to investigate the influence of size, surface charge, and aggregation on particle uptake by skin cells. HaCaT cells are spontaneously immortalized human keratinocytes and are similar to normal keratinocytes with regard to growth and differentiation properties.[44] Flow cytometry (Figure 3) allowed the analysis of a large number of cells and the quantification of cells associated with silica particles (i.e., cells with internalized and/or membrane adsorbed particles), whereas confocal laser scanning microscopy (CLSM, Figure 4) was used to verify particle internalization. The flow cytometry analyses of HaCaT cells incubated for 2 h with the particles revealed that most of the cells were associated with particles, as a marked shift of the sample fluorescence signal with respect to that of control cells was detected.

The fraction of cells associated with silica particles was approximately 90−99% for all samples, independent from the particle size and surface functionalization. The changes in surface charge and hydrodynamic diameter occurring during the transfer of particles to PBS and their dilution in cell culture medium did not impede the uptake of particles by HaCaT cells. Evidently, even if aggregation occurred, the fraction of the small aggregates and nonaggregated particles was

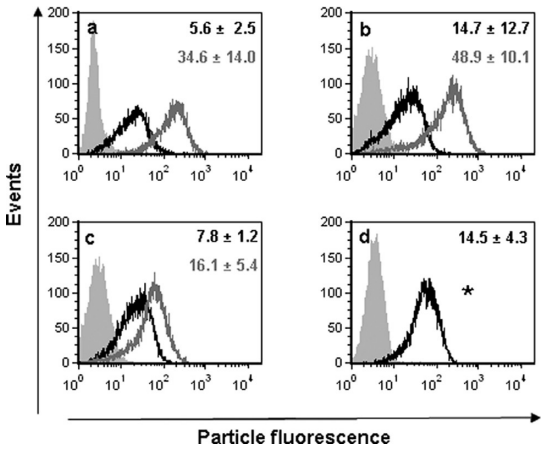

Figure 3. Uptake of SiO_2 particles by HaCaT cells. Cells were incubated with the samples (10 μg/mL, 2 h, 37 °C) SiO_2-42 and APS-SiO_2-42 (a), SiO_2-75 and APS-SiO_2-75 (b), SiO_2-200 and APS-SiO_2-200 (c), SiO_2-300 and APS- SiO_2-300 (d). Cells incubated with nonfunctionalized (black lines) and APS-functionalized (gray lines) SiO_2 particles show a positive particle-related signal with respect to the untreated control cells (filled gray histograms). The averaged (n = 4) relative mean fluorescence intensity (MFI) values are displayed for nonfunctionalized (black) and functionalized (gray) SiO_2 particles. *The analysis of APS-SiO_2-300 samples was not possible because of particle sedimentation.

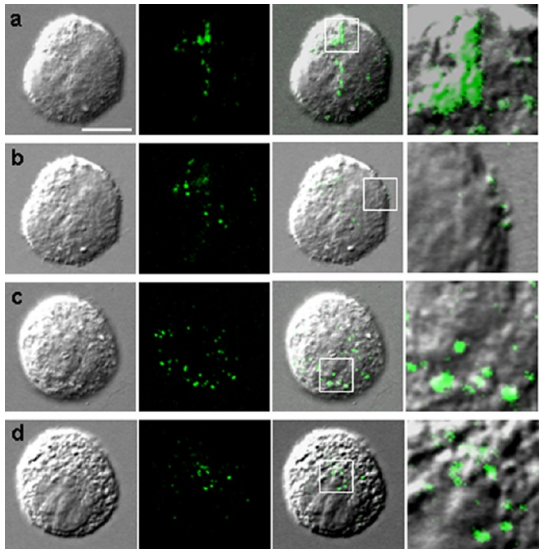

Figure 4. CLSM analysis of HaCaT cells incubated with SiO_2 particles show internalized single particles as well as aggregates. The rows a and b are two different sections of the same cell showing single and aggregated particles of the SiO_2-200 sample; the rows c and d are two different sections of the same cell showing particles of the SiO_2-42 sample accumulated in the cells. The last column shows the 4-fold magnification of the respective boxed areas. An Olympus FV1000 confocal scanning microscope was used to collect z-stacks of single cells (Olympus, Germany). The pictures are a selection of images collected in three independent experiments. Scale bar = 5 μm.

sufficient to reach internalization by almost all incubated cells. HaCaT cells treated with APS-functionalized particles displayed stronger fluorescence shifts than cells incubated with nonfunctionalized negatively

charged particles of the same size. This observation confirms the hypothesis that the interactions of positively charged particles with the negative charges on cell membrane would facilitate their internalization.[37] Obviously, the positive surface charge of the APS-functionalized particles significantly promoted the cellular uptake, despite of the fact that a large fraction of the APS-functionalized particles was aggregated (see Figure 2). Nevertheless, the shift between SiO_2-200 and APS-SiO_2-200 samples was smaller compared to that observed for the samples with smaller TEM diameters (i.e., 75 ± 6 or 42 ± 3 nm). This means that, in the case of the 190 ± 9 nm diameter particles, the APS functionalization had a less positive effect with regard to cellular internalization due to the big size of particle aggregates. In the case of the APS-SiO_2-42 and APS-SiO_2-75 samples, the aggregates with low aggregation number ($\leq$10) are still small enough to be taken up by the cells. For all these small aggregates the uptake is enhanced by the APS functionalization. In the case of SiO_2-200 and APS-SiO_2-200 samples, the diameter of the primary particles is already large (190 ± 9 nm) and close to the size limit for receptor-mediated endocytosis.[45] Consequently, for the APS-SiO_2-200 sample only nonaggregated particles are available for cellular uptake, which results in a significantly smaller shift between the flow cytometry histograms of APS-SiO_2-200 and nonfunctionalized SiO_2-200 particles.

Confocal laser scanning microscopy (CLSM) studies have been performed in order to confirm the intracellular uptake of SiO_2 particles (Figure 4). The same HaCaT cells which were analyzed by means of flow cytometry have been imaged by confocal fluorescence microscopy. Detached from the growing surface, HaCaT cells have a spherical shape and a diameter of approximately 12−18 μm. The CLSM analysis of the cells, by *z*-stacks with 1 μm steps, allowed us to scan several cell cross sections and to verify the presence of particles within intracellular areas. The CLSM images confirmed the intracellular uptake of silica particles independent of their size and surface functionalization (Figure 4). Rapidly proliferating cell lines often possess uptake mechanisms which are different from those of the deriving primary cells. It has been reported that HaCaT cells can internalize substances and particulate material by means of macropinocytosis and that they are able to internalize dextran colloids with a size of 20 μm.[46] In the case of silica particles, nonaggregated particles (Figure 4, B) as well as small aggregates (Figure 4 A) were observed in cells incubated with SiO_2-200 particle dispersions. However, these aggregates were never larger than a few hundred nanometers. Even if the nanoparticles have a size which is below the resolution limit of a conventional optical microscope, diffused fluorescence associated with single particles was rarely observed within cells. We rather observed fluorescent spots close to the cell membrane and in the perinuclear region (Figure 4C,D). The spots have a regular shape and a size of approximately 200 nm, which is indicative for particle accumulation in endosomal vesicles and consequently for an endocytotic internalization pathway.[45] This finding leads us to the hypothesis that HaCaT cells preferentially internalize particle aggregates in the size regime of about 200 nm or alternatively that single particles accumulate in specific areas of the plasma membrane prior to being internalized into endosomes which have a diameter size of about 200 nm. Endocytosis has been described as the preferential internalization mechanism for several particle types.[45] However, it is still unclear if an interaction with a receptor is always required, for example , *via* serum proteins adsorbed on the particle surface. In the present experiments HaCaT cells were incubated with silica particles in serum-free medium. Therefore, we can exclude that the interaction of particles with the cell membrane takes place *via* the binding of serum proteins adsorbed on a particle surface to a specific receptor.

Surface Functionalization, Size, And Aggregation Influence the Uptake of Silica Particles by Primary Skin Cells. It has been shown that, when the skin barrier is partially damaged, particles and macromolecules can bypass the horny layer (stratum corneum) and come in direct contact with the first layers of keratinocytes.[14,47] Nevertheless, the first cell layers of the epidermis represent a further barrier to particle translocation into the viable tissue, being connected by means of tight junctions. Therefore, particles should be smaller than the gaps between the tight junctions (~6 nm) or actively internalized by cells in order to penetrate into skin. This is, for example, the case of dendritic cells of the skin immune system.[47] The cellular uptake of particles varies strongly depending on the cell type. In particular, subsets of cells of the skin immune system are specialized in the uptake of pathogens and can internalize proteins and other antigens by means of endocytosis, macropynocytosis, and phagocytosis.[48] We have therefore focused our interest on epidermis cells (ECs) and on Langerhans cells (LCs). Keratinocytes are the most represented cells of the epidermis (90%), whereas the LCs represent approximately 3−5% of all epidermis cells.[6,49] The flow cytometry analysis of freshly isolated skin cells incubated with differently sized silica particles showed that the size of the primary particles, the degree of aggregation, and the surface charge significantly influenced particle uptake. Remarkably, different uptake abilities between ECs and LCs were measured. In general, LCs showed higher mean fluorescence intensity (MFI) values than ECs incubated with the same silica particles, indicating that LCs were more prone than ECs to internalize particles (see Figure 5).

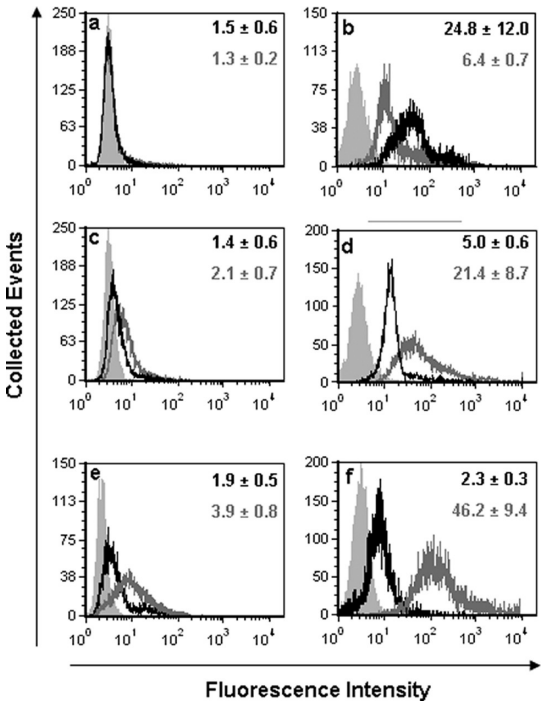

Figure 5. Association of SiO_2 particles with primary epidermis and Langerhans cells. After incubation of cells with samples SiO_2-200 (a), APS-SiO_2-200 (b), SiO_2-75 (c), APS-SiO_2-75 (d), SiO_2-42 (e), and APS-SiO_2-42 (f) (10 μg/mL, 2 h, 37 °C), association of SiO_2 particles with freshly isolated ECs (a,c,e) and LCs (b,d,f) were analyzed by means of flow cytometry. Cells incubated with nonfunctionalized (open black lines) and APS-functionalized (open gray lines) SiO_2 particles were compared with untreated control cells (filled gray histograms). The averaged (n = 4) relative mean fluorescence intensity (MFI) values are displayed for nonfunctionalized (black) and functionalized (gray) SiO_2 particles. The results show that LCs were more prone than ECs to particle uptake and that APS-functionalization promoted the association of silica particles with cells.

This was mostly evident in the case of the samples with a primary particle size of 190 ± 9 nm. In fact, primary ECs incubated with fluorescently labeled SiO_2-200 and APS-SiO_2-200 particles gave the same shift as control cells (Figure 5a), which means that no or negligible particle uptake took place. On the contrary, the signal of LCs incubated with the same silica particles was strongly shifted with respect to control cells (Figure 5b). Thus, the extent to which size and aggregation influence particle cellular uptake varies with the type of the investigated cells. Primary cells feature different endocytosis mechanisms depending on their physiological role. Dendritic cells, such as LCs, are able to internalize pathogens with sizes in the micrometer range by means of phagocytosis, whereas keratinocytes internalize by means of endocytosis, which is limited to material with a size of about 200 nm.[45] The present results indicate that silica nanoparticles and their aggregates are internalized by means of different uptake mechanisms depending on their size. HaCaT cells and LCs can internalize particles with a diameter of 200 nm and larger aggregates by means of phagocytosis or macropinocytosis, whereas ECs can uptake only particles with sizes below 200 nm most likely by means of endocytosis.

The uptake of silica particles by both cell types is found to be enhanced when the particle surface was functionalized with positively charged ligands. The fluorescence intensity signal of ECs incubated with positively charged APS-SiO_2-75 and APS-SiO_2-42 nm particles is higher than that of cells incubated with the nonfunctionalized negatively charged particles. For example, in the case of the APS-SiO_2-42 sample, the relative MFI values were of 2.9 ± 0.8 and 1.9 ± 0.5, respectively (see Figure 5e). The extent of particle association with LCs was also positively influenced by the APS-functionalization, with the exception of 190 ± 9 nm particles (Figure 5b), where the high tendency of APS-functionalized particles to form aggregates resulted in a reduction of the cellular uptake. The fact that the functionalization of the particle surface with APS molecules enhanced the uptake of the smaller particles (75 ± 6 and 42 ± 3 nm), but not that of the 190 ± 9 nm particles, can be easily explained by the fact that the APS-SiO_2-200 sample formed aggregates with a larger size than those formed by APS-SiO_2-75 and APS-SiO_2-42 samples (see Table 4). These are evidently too big to be internalized even by LCs. Therefore, even if samples APS-SiO_2-75 and APS-SiO_2-42 have a similar aggregation number than APS-SiO_2-200 sample (Figure 2), the extent of cellular uptake was different. These results show that even LCs are less prone to internalize particles or aggregates with diameters significantly larger than 200 nm. Consequently, for the APS-SiO_2-200 sample the negative effects of aggregation on the cellular uptake was more important than the enhanced internalization achieved by means of particle surface functionalization.

These data support the general observation that a positive charge on the particle surface enhances their electrostatic interactions with the cell membrane and favors their internalization.[50] However, particle colloidal stability, which is correlated to particle surface charge, strongly affected particle aggregation and cellular uptake. In addition, we found that LCs internalized particles more efficiently than keratinocytes, representing thereby a significant particle-scavenging mechanism as well as a possible target for intended transcutaneously applied particles

Translocation of Amorphous Silica Particles through the Skin Barrier. Investigations on nanoparticle interactions with physiological body barriers are a matter of research for both safety and drug delivery purposes. Under physiological conditions, particles need to bypass barriers, such as films made of lipids and proteins as well as cell layers sealed by tight junctions, before they can enter body compartments and interfere with biological processes. These barriers act as physical impediment but might also interact with the particles

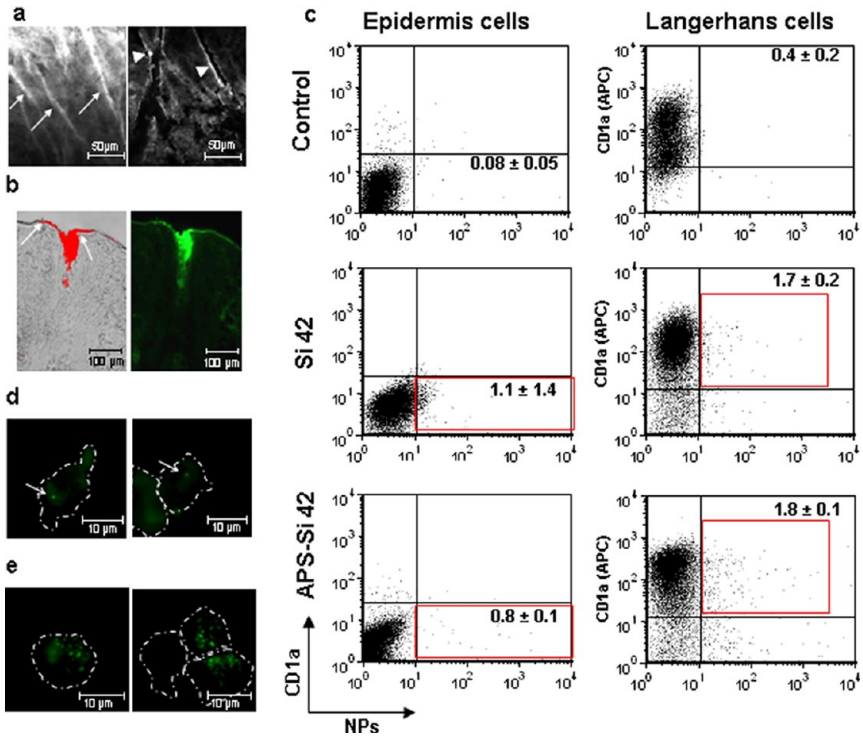

Figure 6. Skin penetration of SiO_2-42 and APS-SiO_2-42 particles after topical application on cyanoacrylate-stripped skin explants. After application of the particle dispersion (0.4%), skin was incubated in a humidified chamber at 37 °C for 16 h. (a) Representative images are shown of particle distribution on skin surface monitored by means of CLSM. Arrows show particles accumulated in skin furrows and triangles particles on the hair shaft. (b) Skin sections showing the accumulation of silica particles in a hair follicle canal. Arrows show the penetration of the nanoparticles in the stratum corneum around the hair follicle orifice. (c) ECs (CD1a negative) and LCs (CD1a positive) isolated from skin topically treated with SiO_2-42 and APS-SiO_2-42 samples were analyzed by means of flow cytometry. The fractions of particle-positive cells (boxed areas) are reported as an average of three independent experiments (three different donors). Representative fluorescence microscopy images showing that ECs (d) are associated with a few particles (arrows), whereas LCs (e) take up several silica nanoparticles.

and change their surface, for example, by protein adsorption. To elucidate the effects of size and surface functionalization on particle penetration into skin, human skin explants have been used to investigate the distribution of particles on the skin surface, their penetration within the hair follicle canals, and their translocation across the horny layer into the epidermis. Prior to the topical application of the silica particles, skin explants were treated with a single cyanoacrylate skin surface stripping (CSSS) in order to partially remove sebum and other impurities from the hair follicle orifices and improve their accessibility to particle penetration. In fact, in excised skin the hair follicle orifices are often clogged and have a smaller volume due to the loss of the physiological skin elasticity. Therefore, in the case of excised skin, the CSSS pretreatment represents a suitable way to get closer to the *in vivo* situation where most hair follicles are accessible to particles. The analysis of the skin surface by confocal laser microscopy showed that silica particles accumulated mostly in skin furrows (Figure 6a, arrows), in the hair follicle orifices, and also on the hair shafts (Figure 6a, arrowheads).

Similar to other types of nanosized spheres,[13,51] silica particles penetrated also into the hair follicle canals, as visualized in the skin sections. In the case of 42 ± 3 nm silica particles, we also noticed particle-associated fluorescence intensity within the SC (Figure 6b). This is particularly evident in the areas near the hair follicle openings, where the particles were predominantly accumulated (Figure 6b, arrows). The low resolution of a conventional fluorescence microscope did not allow a clear identification of particles within the keratinocyte layers or in the dermis. Therefore, to detect nanoparticles which were translocated through the stratum corneum and had been internalized by keratinocytes and LCs, we performed an enzymatic digestion of the skin and isolated the cells of the epidermal layers. LCs were then separated from epidermal cells by means of magnetic sorting of cells expressing the cluster of differentiation CD1c, as explained in the Materials and Method section. Cell flow cytometry analyses as well as the fluorescence microscopy images revealed that only SiO_2-42 and APS-SiO_2-42 nanoparticles, but not the 75 ± 6 nm samples had translocated to the epidermis and were associated to ECs and LCs. Figure 6c shows a representative dot plot analysis for the SiO_2-42 and the APS-SiO_2-42 samples in comparison to untreated control cells. Small but significant fractions of LCs ($CD1a^+$) and ECs ($CD1a^-$)

were found to be associated with silica particles. More precisely, the ratios of particle-positive LCs detected in the skin of three different donors were 1.7 ± 0.2% and 1.8 ± 0.1% for samples SiO_2-42 and APS-SiO_2- 42, respectively. In the case of ECs, the ratios of particle-positive cells were 1.1 ± 1.4% and 0.8 ± 0.1% for samples SiO_2-42 and APS-SiO_2-42, respectively. Taking into account that the human epidermis has approximately 600 000 cells per square centimeter and that LCs represent 4% of them, we can assume that in one square centimeter of treated skin approximately 6000 keratinocytes and 400 LCs were associated with SiO_2-42 particles. The APS-functionalization, despite enhancing particle uptake *in vitro*, had no significant influence on particle cellular uptake after topical application on skin explants. The fluorescence microscopy analysis of the cells revealed only a few fluorescent spots in most of the positive keratinocytes, whereas several spots were visible within the positive LCs (Figure 6d,e). This finding supports the observations of the *in vitro* uptake experiments, showing the superior uptake ability of LCs. The fact that the particle uptake by cells in skin explant experiments is strongly reduced compared to cellular uptake *in vitro* is due predominantly to the efficiency of the stratum corneum as a barrier. Nanoparticles applied on the skin surface have to bypass several layers of densely packed corneocytes and extracellular lipids before they can interact with the subjacent layers of living skin cells, whereas in the *in vitro* conditions the investigated nanoparticles came directly into contact with the cells.

One possibility for nanoparticles to enter the viable epidermis is to get actively internalized by the cells of the epidermis. LCs form a close network of cells surveying against the entry of pathogens. They are able to collect any encountered foreign antigen initiating or modulating an immune response.[45] In the present study, we demonstrate that small amounts of 42 ± 3 nm silica nanoparticles can penetrate across a slightly damaged skin barrier after topical application and are taken-up especially by LCs. Similar results were obtained in a previous work with commercially available negatively charged polystyrene nanoparticles.[12] It was shown that only 40 nm polystyrene particles, but not 750 or 1500 nm ones, could translocate through the skin barrier of human skin explants and were internalized by LCs. The present work, investigating amorphous silica particles with diameters ranging between 40 and 300 nm, confirms that particle size is a major determinant for the translocation of particles across the SC. Nevertheless, the fraction of LCs found positive for polystyrene nanoparticles was higher (24 ± 12%) than those detected for the silica nanoparticles investigated in the present work (2%), suggesting that besides size other physicochemical parameters like colloidal stability or formability might influence the extent of nanoparticle penetration across the skin barrier. Recently, it has been demonstrated that murine LCs can internalize external antigens by elongating their dendrites between the most apical granulocytes of the epidermis.[47] A dynamic reorganization of the epidermal tight junction between LCs and keratinocytes permitted LCs to extend their dendrites through the tight junction barrier without disruption of the skin barrier. This behavior was associated with activation of LCs, for example, by tape stripping, and would allow the immune system to resist the challenge of possible pathogens. Our present observations, together with these findings, underline the active role of LCs in the translocation of nanosized materials across the skin barrier. Moreover, the storage of particles in the hair follicle canals might last for days, as reported for TiO_2 particles.[52] In the case of amorphous silica particles, CLSM and skin cryosections (Figure 6a,b) showed that SiO_2-42 nm particles stuck on the hair shafts and accumulate in the hair follicle ducts. Therefore, the contact of particles with skin surface *in vivo* might last longer than 16 h, which would increase the number of LCs getting in contact with the accumulated nanoparticles.

The CSSS treatment removes part of the SC and can slightly damage the junctions between the corneocytes, so that the experimental conditions used in this work might not strictly reproduce the penetration conditions of nanoparticles through healthy skin. However, there are several situations or pathological conditions in which the skin barrier is altered. For example, this might occur in the case of sun burn, eczema, atopic dermatitis, and psoriasis. In these special cases, the penetration of nanoparticles through a disrupted skin barrier is more likely to occur.

The present results show that an amorphous silica particle with a size of 42 ± 3 nm can penetrate also across a slightly damaged skin barrier and be internalized by small ratios of skin cells. These results might be improved by increasing the colloidal stability of the particles or varying other parameters such as particle formability. Hence, our findings underscore that deeper knowledge on the physicochemical parameters governing the translocation of nanoparticles to the viable skin is still required.

CONCLUSIONS

Studies on nanoparticle translocation across biological barriers and cellular uptake are of high relevance to understand possible risks associated with particle exposure as well as to explore novel fields of application in diagnostics and therapy. While penetration of solid nanomaterials across intact stratum corneum seems to be very limited, we recently associated moderate barrier disruption by skin surface stripping with an increased likelihood of nanoparticle translocation into the viable tissue using human skin explants as model system. In this study, we found that the surface functionalization of amorphous silica

particles with positively charged groups enhances the cellular uptake by different types of skin cells *in vitro*. On the other hand, the penetration of silica nanoparticles in the skin is clearly size dependent. In fact, we found that human skin can efficiently block the penetration of silica particles of above 75 nm in size, even after mild skin barrier disruption by means of cyanoacrylate biopsy. These experiments on excised human skin underline that particle−skin interactions are even more complex than *in vitro* particle−cell interactions, because they address the question of particle behavior upon contact with the complex multicellular environment of the skin which might critically change particle properties and, as a result, the extent of the cellular uptake. The skin penetration data on silica nanoparticles are in line with previous findings on particle−skin interactions published by our groups[12] but also underscore that different types of nanoparticles possess distinct skin penetration abilities. These findings and the fact that there are numerous pathological conditions in which the skin barrier is disrupted and the skin immune system is activated raise questions on the biodistribution and toxicity of silica nanoparticles upon topical application. In fact, because of the storage properties of the hair follicle canals particle retention or redistribution to other organs might occur. On the other hand, nanoparticle-based targeting of hair follicles and the follicular penetration route might be utilized to improve drug delivery to the skin. Further, the fact that the translocated silica nanoparticles were predominantly internalized by LCs, suggests the feasibility of using nanoparticles to target drugs to this type of cells in order to treat inflammatory skin diseases and optimize transcutaneous vaccination strategies.

MATERIALS AND METHODS

Chemicals. All chemicals (ammonia solution (Merck, p.a. 28−30%), 3-(aminopropyl)triethoxysilane (APS, Aldrich, 97%), ethanol (Riedel-de Haën, puriss. p.a., 99.8%), tetraethoxysilane (TES, Fluka, purum, 98%), fluoresceine isothiocyanate (FITC, Fluka, 99%), and Igepal CO-520 (Sigma-Aldrich, 99%)) were used as received without any further purification. Tetraethoxysilane was distilled before use.

Particles Preparation. The reaction vessels utilized in all reaction steps with silica particles were cleaned before use with hydrofluoric acid (8 vol. %) to remove insoluble deposits from the glass surface. Subsequently, they were copiously rinsed with water. All reaction steps were carried out under exclusion of light to prevent bleaching of fluoresceine.

Synthesis of FITC-Dye Labeled Monodisperse Silica Nanoparticles. The coupling product (FITC-APS) of fluoresceine isothiocyanate (FITC) and 3-(aminopropyl)triethoxysilane (APS) was prepared as described by Imhof *et al.*[53] using a 10-fold excess of APS. The reaction product was used without further purification.

FITC-labeled silica nanoparticle cores with a low polydispersity were prepared in a modified microemulsion synthesis: 51.2 mL of Igepal CO-520 (116 mmol) was dissolved in 900 mL of cyclohexane in a 2000 mL Erlenmeyer flask in an ultrasonic bath. A 5.5 mL portion of the aqueous ammonia solution was added, and the mixture was stirred (600 rpm) for 30 min at 25 °C. A 5.6 mL portion of TES (25.1 mmol) and 2 mL of an ethanolic solution of FITC-APS, with an initial concentration of 6.8 mmol/L FITC, were added, and stirring was continued for another 5 min. This FITC/TES ratio corresponds to a nominal FITC concentration of 17 mmol/L silica assuming 100% conversion of TES and a density of colloidal silica of 2 g/cm^3. Subsequently, the dispersion was stored for 6 days at constant temperature (25 °C) without stirring until the final particle size was reached. The cyclohexane was removed by a rotary evaporator and the particles were purified from nonreacted dye by repeated centrifugation (700 g) and redispersion in 100 mL of ethanol. In the subsequent reaction steps these particles were grown larger by seeded growth.[26−28] In every step the dispersions were diluted to silica volume fractions of 0.5% and the ammonia and water concentrations were kept at 0.69 M NH_3 and 1.56 M H_2O. TES (30 mL, 0.134 M) and optionally FITC-APS in ethanol (1 mL containing 6.8 mmol/L FITC) were added per 1000 mL of dispersion for each step. Up to four additional shells were grown onto the particles. Thereby, the outermost shell is always free of dye, so that any interaction of FITC with the environment can be excluded.

Functionalization of FITC-dye Labeled Silica Nanoparticles with APS. The FITC-labeled silica nanoparticles were functionalized with 3-(aminopropyl)triethoxysilane (APS), as described by van Blaaderen *et al.*[54] The amount of APS was calculated to be sufficient to provide an approximately 2.5 monolayer coating on the silica particles.[55] The area on the nanoparticle surface covered by each organosilane molecule was assumed to be nominally 0.6 nm^2.[56] After the functionalization in ethanol the particles were centrifuged at least five times (700 g) and redispersed in ethanol (final silica concentration: ≤ 5−10 g/L) with the help of an ultrasonic bath (Bandelin Sonorex, RK 512 H 860 W, 5−15 min, 25 °C) in order to remove all residues from the synthesis. The particles were stored in ethanol in an argon atmosphere and under exclusion of light. The concentrations of nanoparticle dispersions are obtained by drying samples with a defined volume and weighing the solid with an analytic balance.

Particles Size and Zeta-Potential. Zeta potential and size distribution of the nanoparticles measurements were performed on a Delsa Nano C of Beckman Coulter. In all DLS measurements the scattering angle was fixed at 165°. The samples were measured after transferring them into water-free ethanol, highly pure water (Milli-Q) with a measured resistance of 18.2 MΩcm, and phosphate buffered saline at pH 7.4 (PBS). Prior to the measurements all nanoparticle dispersions were filtered through a RC 0.2 μm syringe filter (Carl Roth GmbH + Co. KG). The concentration of the samples was 0.05 g/L. Similar measurements were also performed using samples with concentrations of 0.1 g/L and 0.025 of the same nanoparticles, yielding similar results.

Transfer of the Functionalized Silica Nanoparticles from Ethanol to PBS. The transfer processes were carried out under argon and in the dark. Centrifuges tubes (SuperClear PP, VWR collection, 50 mL) are used for all centrifugation steps. A dispersion of silica nanoparticles in ethanol (3−5 mL, c = 5 g/L) was mixed with 40 mL of PBS and centrifuged for 15 h at 700 g (T = 4 °C). The sediment containing the silica nanoparticles was first redispersed in 3 mL of PBS using a plastic spatula, then another 5 mL of PBS were added and the sample was further redispersed by ultrasonication for 30 min (Bandelin Sonorex 102H, 240 W, T = 4−10 °C). Subsequently, the dispersion was centrifuged again (700 g, 4 h, T = 4 °C). The supernatant was removed and the sediment redispersed in PBS by ultrasonication for 30 min (Bandelin Sonorex 102H, 240 W, T = 4−10 °C). It should be noted that a different transfer protocol, comprising the transfer of the silica nanoparticles first into water and subsequently into PBS, shorter centrifugation steps (45 min instead of 4−15 h, as used in the present protocol) at higher acceleration (2800 g instead of 700 g) as well as redispersion in an ultrasonic bath with high power (860 W instead of 240 W) results in lower aggregation. For example, the hydrodynamic diameter of 55 nm silica particles in PBS is at most twice as large as that in water.[23]

Transmission Electron Microscopy. Transmission electron microscopy (TEM) images were recorded using an EM 902A TEM of Philips. The TEM samples were prepared by dipping 400 mesh copper grids coated by an ~15 nm carbon film (Quantifoil) into a dispersion of the nanoparticle samples. The concentration of these dispersions was about 0.5 g/L for size measurements.

Highly diluted dispersions in PBS (0.005 g/L) were used for the statistical analysis of particle aggregation in physiological media by means of TEM imaging, since the formation of particle aggregates might be influenced by drying effects during the preparation of the samples. At least 3800 particles from each of the samples SiO_2-42, SiO_2-75, and SiO_2-200 were analyzed. The 300 nm samples precipitated when redispersed in PBS and were therefore not analyzed. Control experiments by DLS indicate that dilution of the samples does not change the state of aggregation.

Cell Culture and Incubation Conditions. A cell line of human keratinocytes (HaCaT cells, Deutsches Krebsforschungszentrum, Heidelberg, Germany) was cultivated in 75 cm^2 flasks in RPMI 1640 medium supplemented with 4 mM glutamine, 10% fetal calf serum (FCS), 100 μg/mL streptomycin, and 100 I.E./mL penicillin. Cells (passage 30−60) were cultivated at 37 °C in 100% humidity and 5% CO_2 and were seeded in new flasks every 2−3 days. Cells at 80−90% confluency were washed once with PBS, treated with 6 mL of trypsin/EDTA (0.02%, Biochrom, Germany/0.02%, Sigma, Germany) for 5−6 min at 37 °C. Thereafter, trypsin was inactivated with RPMI-1640 medium supplemented with 10% FCS, centrifuged (300 g, 10 min), resuspended in culture medium and seeded into a new flask (approximately 100 000 cells/mL). For the uptake experiments, cells were seeded (approximately 2×10^5 cells/mL) in a 6-well plate and 24 h later particle dispersions in PBS were added to the cells in FCS-free medium. Thus, the dispersions of the nanoparticles in PBS were diluted at a ratio of 1:1000 with RPMI 1640 reaching a final concentration of 10 μg/mL. After 2 h of incubation at 37 °C, 100% humidity, and 5% CO_2, cells were washed twice, trypsinized, and fixed in 2% paraformaldeyde (PFA) prior to the analysis by flow cytometry and confocal fluorescence microscopy.

Fluorescence Microscopy of Cells. Confocal laser scanning microscopy analyses of HaCaT cells were performed with a FluoView FV1000 (Olympus, Germany). The samples were excited by an argon-ion laser (488 nm), and the fluorescence was detected in the region of 550−650 nm. The visualization of particles associated with primary skin cells was accomplished by a BX60F3 Olympus microscope (Hamburg, Germany) using 470−490 nm BP and 550 nm LP filters.

Tissue Samples and Transcutaneous Particle Application. Human skin (retroauricular region, breast, and abdomen) was obtained from healthy volunteers undergoing plastic surgery within 4 to 24 h after surgical excision. Volunteers had signed an informed consent form approved by the Institutional Ethics Committee of the Medical Faculty of the Charité—Universitätsmedizin Berlin (Germany) and in accordance with the ethical rules stated in the Declaration of Helsinki Principles. Skin samples were examined macroscopically and microscopically for tissue damage. Only intact skin explants were used for transcutaneous nanoparticle penetration experiments. Subcutaneous fat was partially removed, leaving about 3−5 mm of adipose tissue. The skin was cut into pieces of at least 4 cm^2 for skin cryosections or 20 cm^2 for cell isolation samples. Square areas of 1 cm^2 and 16 cm^2 were treated with the nanoparticle dispersions leaving safety margins of 0.5 cm to the border of the tissue in order to avoid sideways nonspecific penetration of the tested particles into the tissue. Prior to the application of particles, cyanoacrylate skin surface stripping (CSSS) was performed once using superglue (UHU GmbH, Buehl/Baden, Germany). A droplet of cyanoacrylate glue was deposited onto a clear polyethylene tape (TESA film no. 5529, Beiersdorf, Hamburg, Germany). This material was pressed against the surface of the skin for at least 30 s; the cyanoacrylate polymerized and adhered to the SC. After 20 min the material was gently lifted and peeled from the skin. This treatment removes part of the SC and the follicular casts, that is, the content of the follicular infundibulum, hereby simulating mild barrier disruption which we associated in previous studies with a high likelihood of nanomaterial translocation across the skin barrier.[12]

Dispersions of the nanoparticles in PBS (pH = 7.4) were diluted with PBS to a concentration of 0.5% and sonicated for 3 min before use (Sonorex Super RK102H, Bandelin, Berlin, Germany). Skin samples were stretched on expanded polystyrene sheets, previously covered with aluminum foil and laboratory packaging film, and placed in a humidified chamber, which consisted of a box provided with wet napkin paper and a cover, in order to prevent skin dehydration. A volume of 20 μL/cm^2 was applied on the sampled skin area and the chamber was placed for 16 h in an incubator at 37 °C, 5% CO_2 and 100% humidity. This experimental setup efficiently prevented the evaporation of the particle dispersing phase and the drying of the skin. After incubation, adhesive tape stripping was performed five times to remove the particles that had not penetrated. The skin samples were then processed to obtain cryosections or to isolate epidermis cells as described below.

Confocal Laser Scan Microscopy of Intact Skin Explants. The penetration of silica particles within human skin explants was visualized with a "Stratum" fluorescence confocal laser scanning microscope (CLSM, Optiscan Pty Ltd., Melbourne, Australia). Blue laser light (488 nm) was delivered to a miniaturized confocal scanner *via* an optical fiber. The laser light was focused to a diffraction-limited spot on the skin surface or within the tissue and the emitted fluorescence light was refocused from the focal plane back into the optical fiber by objective lenses. The intensity of this fluorescence signal was measured and an image was generated by scanning the focused spot across the tissue in a raster fashion.

Skin Sections. After incubation with particles, a skin area of 1 cm^2 was excised and split into four blocks which were frozen in liquid nitrogen. Cryosections of 5 μm in thickness were prepared from each block using a microtome (2800 Frigocut-N, Reichert-Jung, Heidelberg, Germany). Cutting was performed with fresh blades from the dermis side toward the epidermis in order to avoid dislocation of particles from the skin surface inside the section. Cryosections from three different donors were analyzed by fluorescence microscopy.

Isolation of Epidermis Cells and MACS Separation of Epidermal CD1c+ Langerhans Cells. Skin samples (16 cm^2) were chopped into 3 mm^2 slices. Skin was digested with Dispase (2.4 U/mL Dispase I, Roche, Germany) over 2.5 h at 37 °C in order to detach the epidermis layers. Trypsin digestion (0.025% trypsin, 1.5 mM $CaCl_2$ in PBS) of the epidermis was then performed over 15 min in order to isolate epidermis cells. Cells were collected after filtration and centrifugation. Subsequently, MACS separation with anti-BDCA-1 (anti-CD1c) antibodies was performed on isolated epidermis cell according to the manufacturer's recommendations (Dendritic Cell Isolation Kit, Miltenyi Biotec, Bergisch Gladbach, Germany). Three different experiments using skin from three different donors were performed for each type of studied particles.

Flow Cytometry. Cells incubated *in vitro* with the studied particles (10 μg/mL, 2 h) as well as epidermal and Langerhans cells isolated from skin explants treated with the silica particles (0.5%, 16 h) were analyzed by flow cytometry using a FACS Calibur and the CellQuest software (Becton Dickinson, Heidelberg, Germany). A total number of 20000 events were recorded. The software FCS-Express 3.1 (De Novo Software, USA) was used to analyze the collected data.

Conflict of Interest: The authors declare no competing financial interest.

Acknowledgment. This work was supported by the Deutsche Forschungsgemeinschaft (DFG) (NANO-SELECT project within SPP 1313). We thank Dr. H. Renz and Prof. Dr. R. J. Radlanski (Department of Craniofacial Developmental Biology, Charité-Universitätsmedizin Berlin, Germany) for the use of their electron microscope.

REFERENCES AND NOTES

1. Fadeel, B.; Garcia-Bennett, A. E. Better Safe than Sorry: Understanding the Toxicological Properties of Inorganic Nanoparticles Manufactured for Biomedical Applications. *Adv. Drug Delivery Rev.* **2010**, *62*, 362–374.

2. Papakostas, D.; Rancan, F.; Sterry, W.; Blume-Peytavi, U.; Vogt, A. Nanoparticles in Dermatology. *Arch. Dermatol. Res.* **2011**, *303*, 533–550.
3. Xia, T.; Kovochich, M.; Nel, A. The Role of Reactive Oxygen Species and Oxidative Stress in Mediating Particulate Matter Injury. *Clin. Occup. Environ. Med.* **2006**, *5*, 817–836.
4. Shvedova, A. A.; Kagan, V. E.; Fadeel, B. Close Encounters of the Small Kind: Adverse Effects of Man-Made Materials Interfacing with the Nano-cosmos of Biological Systems. *Annu. Rev. Pharmacol. Toxicol.* **2010**, *50*, 63–88.
5. Napierska, D.; Thomassen, L. C. J.; Lison, D.; Martens, J. A.; Hoet, P. H. The Nanosilica Hazard: Another Variable Entity. *Part. Fibre Toxicol.* **2010**, *7*, 39–71.
6. Merad, M.; Ginhoux, F.; Collin, M. Origin, Homeostasis and Function of Langerhans Cells and Other Langerin-Expressing Dendritic Cells. *Nat. Rev. Immunol.* **2008**, *8*, 935–947.
7. Lademann, J.; Weigmann, H. J.; Rickmeyer, C.; Barthelmes, H.; Schaefer, H.; Müller, G.; Sterry, W. Penetration of Titanium Dioxide Microparticles in a Sunscreen Formulation into the Horny Layer and the Follicular Orifice. *Skin Pharmacol. Appl. Skin Physiol.* **1999**, *12*, 247–256.
8. Baroli, B.; Ennas, M. G.; Loffredo, F.; Isola, M.; Pinna, R.; Lopez-Quintela, M. A. Penetration of Metallic Nanoparticles in Human Full-Thickness Skin. *J. Invest. Dermatol.* **2007**, *127*, 1701–1712.
9. Cross, S. E.; Innes, B.; Roberts, M. S.; Tsuzuki, T.; Robertson, T. A.; McCormick, P. Human Skin Penetration of Sunscreen Nanoparticles: *In-Vitro* Assessment of a Novel Micronized Zinc Oxide Formulation. *Skin Pharmacol. Physiol.* **2007**, *20*, 148–154.
10. Zhang, L. W.; Monteiro-Riviere, N. A. Assessment of Quantum Dot Penetration into Intact, Tape-Stripped, Abraded and Flexed Rat Skin. *Skin Pharmacol. Phys.* **2008**, *21*, 166–180.
11. Larese, F. F.; D'Agostin, F.; Crosera, M.; Adami, G.; Renzi, N.; Bovenzi, M.; Maina, G. Human Skin Penetration of Silver Nanoparticles through Intact and Damaged Skin. *Toxicology* **2009**, *255*, 33–37.
12. Vogt, A.; Combadiere, B.; Hadam, S.; Stieler, K. M.; Lademann, J.; Schaefer, H.; Autran, B.; Sterry, W.; Blume-Peytavi, U. 40 nm, but not 750 or 1,500 nm, Nanoparticles Enter Epidermal CD1a+ Cells after Transcutaneous Application on Human Skin. *J. Invest. Dermatol.* **2006**, *126*, 1316–1322.
13. Mahe, B.; Vogt, A.; Liard, C.; Duffy, D.; Abadie, V.; Bonduelle, O.; Boissonnas, A.; Sterry, W.; Verrier, B.; Blume-Peytavi, U.; *et al*. Nanoparticle-Based Targeting of Vaccine Compounds to Skin Antigen-Presenting Cells By Hair Follicles and Their Transport in Mice. *J. Invest. Dermatol.* **2009**, *129*, 1156–1164.
14. Mortensen, L. J.; Oberdorster, G.; Pentland, A. P.; DeLouise, L. A. *In Vivo* Skin Penetration of Quantum Dot Nanoparticles in the Murine Model: The Effect of UVR. *Nano Lett.* **2008**, *8*, 2779–2787.
15. Rahman, A.; Seth, D.; Mukhopadhyaya, S. K.; Brahmachary, R. L.; Ulrichs, C.; Goswami, A. Surface Functionalized Amorphous Nanosilica and Microsilica with Nanopores as Promising Tools in Biomedicine. *Naturwissenschaften* **2009**, *96*, 31–38.
16. Ketelson, H. A.; Brook, M. A.; Pelton, R. H. Sterically Stabilized Silica Colloids: Radical Grafting of Poly(methyl methacrylate) and Hydrosilylative Grafting of Silicones to Functionalized Silica. *Polym. Adv. Technol.* **1995**, *6*, 335–344.
17. He, X. X.; Wang, K. M.; Tan, W. H.; Li, J.; Yang, X. H.; Huang, S. S.; Li, D.; Xiao, D. Photostable Luminescent Nanoparticles as Biological Label for Cell Recognition of System Lupus Erythematosus Patients. *J. Nanosci. Nanotechnol.* **2002**, *2*, 317–320.
18. Liu, S. H.; Han, M. Y. Synthesis, Functionalization, and Bioconjugation of Monodisperse, Silica-Coated Gold Nanoparticles: Robust Bioprobes. *Adv. Funct. Mater.* **2005**, *15*, 961–967.
19. Calvert, G. M.; Rice, F. L.; Boiano, J. M.; Sheehy, J. W.; Sanderson, W. T. Occupational Silica Exposure and Risk of Various Diseases: An Analysis Using Death Certificates from 27 States of the United States. *Occup. Environ. Med.* **2003**, *60*, 122–129.
20. So, S. J.; Jang, I. S.; Han, C. S. Effect of Micro/Nano Silica Particle Feeding for Mice. *J. Nanosci. Nanotechnol.* **2008**, *8*, 5367–5371.
21. Sayes, C. M.; Reed, K. L.; Warheit, D. B. Assessing Toxicity of Fine and Nanoparticles: Comparing *In Vitro* Measurements to *In Vivo* Pulmonary Toxicity Profiles. *Toxicol. Sci.* **2007**, *97*, 163–180.
22. Nabeshi, H.; Yoshikawa, T.; Matsuyama, K.; Nakazato, Y.; Matsuo, K.; Arimori, A.; Isobe, M.; Tochigi, S.; Kondoh, S.; Hirai, T.; *et al*. Systemic Distribution, Nuclear Entry and Cytotoxicity of Amorphous Nanosilica Following Topical Application. *Biomaterials* **2011**, *32*, 2713–2724.
23. Graf, C.; Gao, Q.; Schütz, I.; Noufele, C. N.; Ruan, W.; Posselt, U.; Korotianskiy, E.; Nordmeyer, D.; Rancan, F.; Hadam, S.; *et al*. Surface Functionalization of Silica Nanoparticles Supports Colloidal Stability in Physiological Media and Facilitates Internalization in Cells. *Langmuir* **2012**, *28*, 7598–7613.
24. Okuda-Shimazaki, J.; Takaku, S.; Kanehira, K.; Sonezaki, S.; Taniguchi, A. Effects of Titanium Dioxide Nanoparticle Aggregate Size on Gene Expression. *Int. J. Mol. Sci.* **2010**, *11*, 2383–2392.
25. Stöber, W.; Fink, A.; Bohn, E. Controlled Growth of Monodisperse Silica Spheres in Micron Size Range. *J. Colloid Interface Sci.* **1968**, *26*, 62–69.
26. Bogush, G. H.; Zukoski, C. F. Uniform Silica Particle Precipitation: An Aggregative Growth Model. *J. Colloid Interface Sci.* **1991**, *142*, 19–34.
27. Philipse, A. P. Quantitative Aspects of the Growth of (Charged) Silica Spheres. *Coll. Pol. Sci.* **1988**, *266*, 1174–1180.
28. van Blaaderen, A.; van Geest, J.; Vrij, A. Monodisperse Colloidal Silica Spheres from Tetraalkoxysilanes: Particle Formation and Growth Mechanism. *J. Colloid Interface Sci.* **1992**, *154*, 481–501.
29. Mailänder, V.; Landfester, K. Interaction of Nanoparticles with Cells. *Biomacromolecules* **2009**, *10*, 2379–2400.
30. Kittler, S.; Greulich, C.; Gebauer, J. S.; Diendorf, J.; Treuel, L.; Ruiz, L.; Gonzalez-Calbet, J. M.; Vallet-Regi, M.; Zellner, R.; Koller, M.; *et al*. The Influence of Proteins on the Dispersability and Cell-Biological Activity of Silver Nanoparticles. *J. Mater. Chem.* **2010**, *20*, 512–518.
31. Wiogo, H. T. R.; Lim, M.; Bulmus, V.; Yun, J.; Amal, R. Stabilization of Magnetic Iron Oxide Nanoparticles in Biological Media by Fetal Bovine Serum (FBS). *Langmuir* **2011**, *27*, 843–850.
32. Verwey, E. J. W.; Overbeek, J. T. G. *Theory of the Stability of Lyophobic Colloids*; Elsevier: New York, 1948.
33. Derjaguin, B.; Landau, L. Theory of the Stability of Strongly Charged Lyophobic Sols and of the Adhesion of Strongly Charged Particles in Solutions of Electrolytes. *Acta Physicochim. URSS* **1941**, *14*, 663–667.
34. Morrison, I. D. Criterion for Electrostatic Stability of Dispersions at Low Ionic-Strength. *Langmuir* **1991**, *7*, 1920–1922.
35. Holthoff, H.; Egelhaaf, S. U.; Borkovec, M.; Schurtenberger, P.; Sticher, H. Coagulation Rate Measurements of Colloidal Particles by Simultaneous Static and Dynamic Light Scattering. *Langmuir* **1996**, *12*, 5541–5549.
36. Lin, M. Y.; Lindsay, H. M.; Weitz, D. A.; Ball, R. C.; Klein, R.; Meakin, P. Universal Reaction-Limited Colloid Aggregation. *Phys. Rev. A* **1990**, *41*, 2005–2020.
37. Wilhelm, C.; Gazeau, F.; Roger, J.; Pons, J. N.; Bacri, J. C. Interaction of Anionic Superparamagnetic Nanoparticles with Cells: Kinetic Analyses of Membrane Adsorption and Subsequent Internalization. *Langmuir* **2002**, *18*, 8148–8155.
38. Mahtab, F.; Yu, Y.; Lam, J. W. Y.; Liu, J.; Zhang, B.; Lu, P.; Zhang, X.; Tang, B. Z. Fabrication of Silica Nanoparticles with Both Efficient Fluorescence and Strong Magnetization, and Exploration of Their Biological Applications. *Adv. Funct. Mater.* **2011**, *21*, 1733–1740.
39. Kim, S.-I.; Pham, T. T.; Lee, J.-W.; Roh, S.-H. Multi-Amine-Grafted SBA-15 Spherical Nanoparticles for the Adsorption of Proteins. *J. Nanosci. Nanotechnol.* **2010**, *10*, 3425–3429.

40. Mao, Z.; Wan, L.; Hu, L.; Ma, L.; Gao, C. Tat Peptide Mediated Cellular Uptake of SiO_2 Submicron Particles. *Colloid. Surface. B* **2010**, *75*, 432–440.
41. Kumar, R.; Roy, I.; Ohulchanskky, T. Y.; Vathy, L. A.; Bergey, E. J.; Sajjad, M.; Prasad, P. N. *In Vivo* Biodistribution and Clearance Studies Using Multimodal Organically Modified Silica Nanoparticles. *ACS Nano* **2010**, *4*, 699–708.
42. Chen, Z. P.; Xu, R. Z.; Zhang, Y.; Gu, N. Effects of Proteins from Culture Medium on Surface Property of Silanes-Functionalized Magnetic Nanoparticles. *Nanoscale Res. Lett.* **2009**, *4*, 204–209.
43. Asenath-Smith, E.; Chen, W. How To Prevent the Loss of Surface Functionality Derived from Aminosilanes. *Langmuir* **2008**, *24*, 12405–12409.
44. Boukamp, P.; Petrussevska, R. T.; Breitkreutz, D.; Hornung, J.; Markham, A.; Fusenig, N. E. Normal Keratinization in a Spontaneously Immortalized Aneuploid Human Keratinocyte Cell-Line. *J. Cell Biol.* **1988**, *106*, 761–771.
45. Conner, S. D.; Schmid, S. L. Regulated Portals of Entry into the Cell. *Nature* **2003**, *422*, 37–44.
46. Morhenn, V. B.; Lemperle, G.; Gallo, R. L. Phagocytosis of Different Particulate Dermal Filler Substances by Human Macrophages and Skin Cells. *Dermotol. Surg.* **2002**, *28*, 484–490.
47. Kubo, A.; Nagao, K.; Yokouchi, M.; Sasaki, H.; Amagai, M. External Antigen Uptake by Langerhans Cells with Reorganization of Epidermal Tight Junction Barriers. *J. Exp. Med.* **2009**, *206*, 2937–2946.
48. Coombes, J. L.; Robey, E. A. Dynamic Imaging of Host-Pathogen Interactions *In Vivo*. *Nat. Rev. Immunol.* **2010**, *10*, 353–364.
49. Valladeau, J.; Saeland, S. Cutaneous Dendritic Cells. *Semin. Immunol.* **2005**, *17*, 273–283.
50. Leroueil, P. R.; Hong, S. Y.; Mecke, A.; Baker, J. R.; Orr, B. G.; Banaszak Holl, M. M. Nanoparticle Interaction with Biological Membranes: Does Nanotechnology Present a Janus Face?. *Acc. Chem. Res.* **2007**, *40*, 335–342.
51. Rancan, F.; Papakostas, D.; Hadam, S.; Hackbarth, S.; Delair, T.; Primard, C.; Verrier, B.; Sterry, W.; Blume-Peytavi, U.; Vogt, A. Investigation of Polylactic Acid (PLA) Nanoparticles as Drug Delivery Systems for Local Dermatotherapy. *Pharm. Res.* **2009**, *26*, 2027–2036.
52. Lademann, J.; Richter, H.; Teichmann, A.; Otberg, N.; Blume-Peytavi, U.; Luengo, J.; Weiss, B.; Schaefer, U. F.; Lehr, C. M.; Wepf, R.; *et al.* Nanoparticles—An Efficient Carrier for Drug Delivery into the Hair Follicles. *Eur. J. Pharm. Biopharm.* **2007**, *66*, 159–164.
53. Imhof, A.; Megens, M.; Engelberts, J. J.; de Lang, D. T. N.; Sprik, R.; Vos, W. L. Spectroscopy of Fluorescein (FITC) Dyed Colloidal Silica Spheres. *J. Phys. Chem. B* **1999**, *103*, 1408–1415.
54. van Blaaderen, A.; Vrij, A. Synthesis and Characterization of Monodisperse, Colloidal, Organo-Silica Spheres. *J. Colloid Interface Sci.* **1993**, *156*, 1–18.
55. Westcott, S. L.; Oldenburg, S. J.; Lee, T. R.; Halas, N. J. Formation and Adsorption of Clusters of Gold Nanoparticles onto Functionalized Silica Nanoparticle Surfaces. *Langmuir* **1998**, *14*, 5396–5401.
56. Waddell, T. G.; Leyden, D. E.; DeBello, M. T. The Nature of Organosilane to Silica−Surface Bonding. *J. Am. Chem. Soc.* **1981**, *103*, 5303–5307.